THE JOURNAL OF BIOLOGICAL CHEMISTRY VOL. 282, NO. 43, pp. 31534–31541, October 26, 2007

Structural and Functional Studies of the Abundant Tegument Protein ORF52 from Murine Gammaherpesvirus 68*

Received for publication, July 10, 2007 Published, JBC Papers in Press, August 15, 2007, DOI 10.1074/jbc.M705637200

Jordi Benach[‡], Lili Wang[§1], Yang Chen[‡1], Chi Kent Ho[¶], Shaoying Lee[‖], Jayaraman Seetharaman[‡], Rong Xiao[¶], Thomas B. Acton[¶], Gaetano T. Montelione[¶], Hongyu Deng[§‖], Ren Sun[2], and Liang Tong[‡3]**

*From the [‡]Department of Biological Sciences, Northeast Structural Genomics Consortium, Columbia University, New York, New York 10027, the [§]Center for Infection and Immunity, National Laboratory of Biomacromolecules, Institute of Biophysics, Chinese Academy of Sciences, Beijing 100101, China, the [¶]Center for Advanced Biotechnology and Medicine and Department of Molecular Biology and Biochemistry, Northeast Structural Genomics Consortium, Rutgers University, Piscataway, New Jersey 08854, and the [‖]School of Dentistry and the **Department of Molecular and Medical Pharmacology, University of California, Los Angeles, California 90095*

The tegument is a layer of proteins between the nucleocapsid and the envelope of herpesviruses. The functions of most tegument proteins are still poorly understood. In murine gammaherpesvirus 68, ORF52 is an abundant tegument protein of 135 residues that is required for the assembly and release of infectious virus particles. To help understand the molecular basis for the function of this protein, we have determined its crystal structure at 2.1 Å resolution. The structure reveals a dimeric association of this protein. Interestingly, an N-terminal α-helix that assumes different conformation in the two monomers of the dimer mediates the formation of an asymmetrical tetramer and contains many highly conserved residues. Structural and sequence analyses suggest that this helix is more likely involved in interactions with other components of the tegument or nucleocapsid of the virus and that ORF52 functions as a symmetrical dimer. The asymmetrical tetramer of ORF52 may be a "latent" form of the protein, when it is not involved in virion assembly. The self-association of ORF52 has been confirmed by co-immunoprecipitation and fluorescence resonance energy transfer experiments. Deletion of the N-terminal α-helix, as well as mutation of the conserved Arg[95] residue, abolished the function of ORF52. The results of the functional studies are fully consistent with the structural observations and indicate that the N-terminal α-helix is a crucial site of interaction for ORF52.

Herpesviruses are large, enveloped viruses that carry a double-stranded DNA genome of ~110–230 kb. Three subfamilies belong to the *Herpesviridae*: alpha-, beta-, and gammaherpesviruses. A unique feature of these viruses is the presence of a tegument layer between the nucleocapsid and the glycoprotein envelope. The tegument is composed predominantly of proteins. Tegument proteins of alpha-, beta-, and gammaherpesviruses have been found to be involved in at least three essential functions in viral replication: (i) the assembly and egress of virions (1–3); (ii) the entry of virions into naive cells, including the translocation of nucleocapsids to the nucleus; and (iii) other effects during the immediate-early phase of infection, including the transactivation of viral immediate-early genes and the possible modulation of host cell gene expression, innate immune mechanisms, and signal transduction (3–7). Recently, proteins in the tegument of various herpesviruses have been identified with the development of mass spectrometry technology (8–13). However, the functions of many tegument proteins have not been defined.

Gammaherpesviruses can infect and establish latency in lymphocytes and cause malignancies, especially in immunocompromised patients (14). Murine gammaherpesvirus 68 (MHV-68)[4] is a natural pathogen of wild rodents (15–17). It is related to human Kaposi's sarcoma-associated virus and Epstein-Barr virus (18–20), and its infection in mice has been developed as an animal model for investigating the biology and pathogenesis of gammaherpesviruses in humans (21). The functions of many MHV-68 proteins can be studied in the context of viral infection by mutagenesis, taking advantage of the herpesvirus genome cloned as bacterial artificial chromosomes (22–26). Although the major proteins in tegument of the gammaherpesviruses have been reported, little is known about the structure and function of these tegument proteins (8, 12).

MHV-68 *ORF52* encodes a capsid-associated tegument protein that is present in abundance in virions (8). It is a highly expressed gene with true late kinetics, activated after viral DNA replication (27, 28). This protein is well conserved among the gammaherpesviruses (Fig. 1), but a homolog has not been found in the alpha- and betaherpesviruses. A number of tegument proteins including ORF52 are unique to each subfamily of herpesvirus and may have distinct roles in the formation and egress of virions (1, 29, 30). Mutation of *ORF52* in the MHV-68/BAC genome leads to arrest at the lytic phase of infection after viral

* This work was supported by Grant U54 GM074958 from the Protein Structure Initiative of the NIGMS, National Institutes of Health, by National Institutes of Health Grant R01 DE015752, and by National Protein Project Grant 2006CB910901. The costs of publication of this article were defrayed in part by the payment of page charges. This article must therefore be hereby marked "*advertisement*" in accordance with 18 U.S.C. Section 1734 solely to indicate this fact.

The atomic coordinates and structure factors (code 2OA5) have been deposited in the Protein Data Bank, Research Collaboratory for Structural Bioinformatics, Rutgers University, New Brunswick, NJ (http://www.rcsb.org/).

[1] These authors contributed equally to this work.

[2] To whom correspondence may be addressed. Tel.: 310-794-5557; Fax: 310-794-5123; E-mail: rsun@mednet.ucla.edu.

[3] To whom correspondence may be addressed. Tel.: 212-854-5203; Fax: 212-865-8246; E-mail: ltong@columbia.edu.

[4] The abbreviations used are: MHV, murine gammaherpesvirus; MOPS, 4-morpholinepropanesulfonic acid; HA, hemagglutinin; CFP, cyan fluorescent protein; YFP, yellow fluorescent protein.

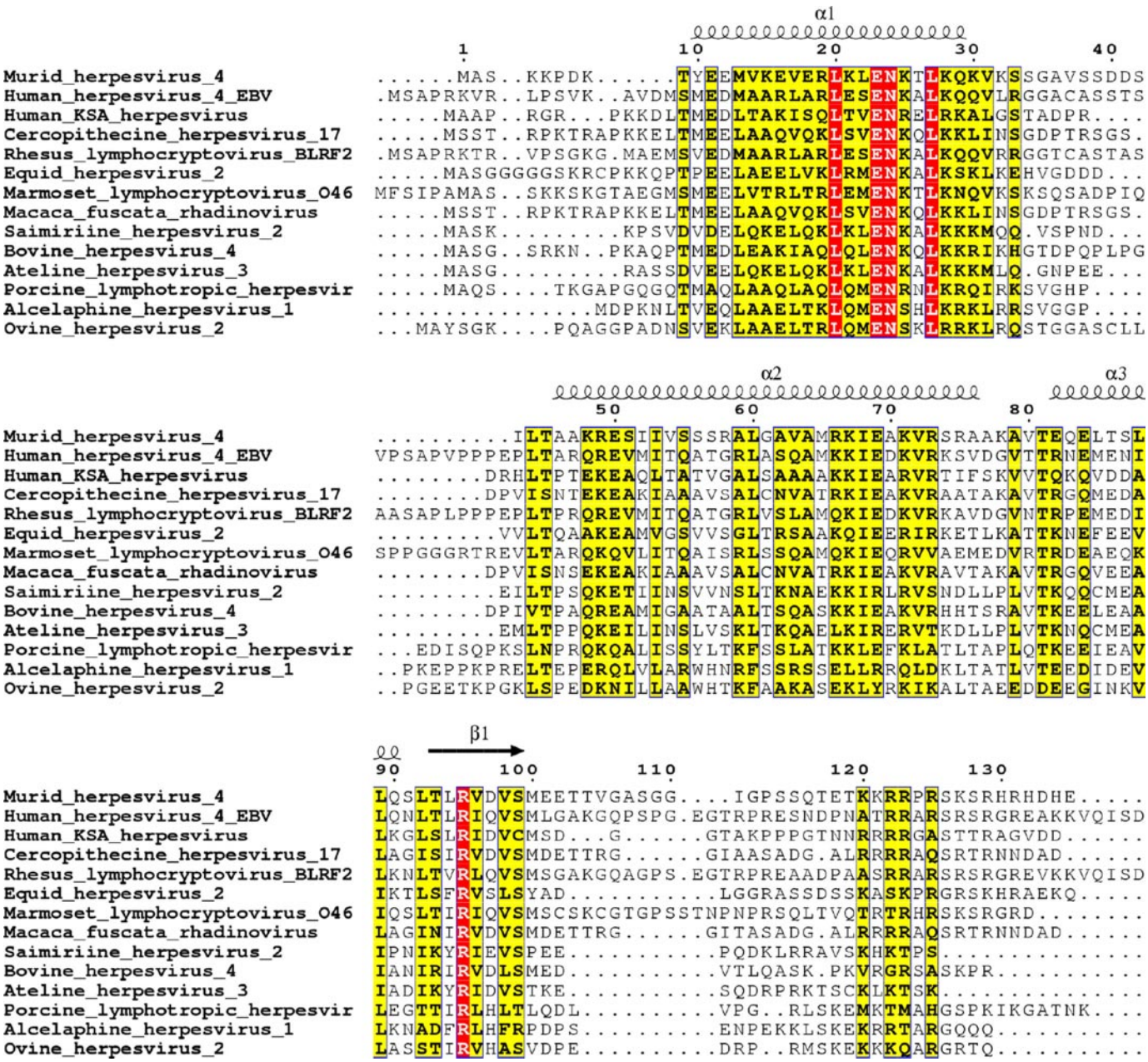

FIGURE 1. **Sequence alignment of herpesvirus ORF52 proteins.** Strictly conserved and conservatively substituted residues are colored with *red* and *yellow backgrounds*, respectively. The secondary structure elements of ORF52 are shown at the *top*, with coils representing α-helices and the *arrow* representing the β-strand. Produced with ESPript (42).

genome replication, late gene expression, viral DNA cleavage/packaging, and nucleocapsid assembly in the nucleus but prior to complete virion tegumentation and envelopment in the cytoplasm and egress of infectious virions from the cell (31). Partially tegumented capsids produced by the *ORF52-null* mutant contain conserved capsid proteins, the ORF64 and ORF67 tegument proteins, but virtually no ORF45 tegument protein. Enhanced green fluorescent protein fusions to ORF52 localize in the cytoplasm to a distinct compartment reminiscent of the secretory pathway (31). ORF52 is essential for the tegumentation and egress of infectious MHV-68 particles in the cytoplasm, suggesting an important function in gammaherpesvirus virion morphogenesis.

To understand the molecular mechanism for the biological functions of ORF52, we have determined the crystal structure of this protein at 2.1 Å resolution. The structure reveals a dimeric association of this protein, except that the N-terminal α-helix does not obey the symmetry of the dimer. This helix contains many highly conserved residues and is more likely involved in interactions with other components of the tegument or nucleocapsid of the virus. We have confirmed the self-association of ORF52 by co-immunoprecipitation experiments. Deletion of this N-terminal α-helix, as well as mutation of the conserved Arg^{95} residue, abolished the function of ORF52.

MATERIALS AND METHODS

Expression and Purification of ORF52—The production of ORF52 protein was carried out using the high throughput protein production platform of the Northeast Structural Genomics

Consortium (32). ORF52 corresponds to Northeast Structural Genomics Consortium target MhR28B (www.nesg.org). A truncated portion of the gene *ORF52* from murine herpesvirus (68 strain WUMS) encoding residues 1–102 was cloned into a pET21 (Novagen) derivative, generating plasmid pMhR28B-21.3. The resulting recombinant protein contains eight nonnative residues (LEHHHHHH) at the C terminus. The construct was sequence-verified by standard DNA sequence analysis.

Escherichia coli BL21 (DE3) pMGK cells, a rare codon enhanced strain, were transformed with pMhR28B-21.3. A single isolate was cultured in MJ9 minimal medium (33) supplemented with selenomethionine, lysine, phenylalanine, threonine, isoleucine, leucine, and valine for the production of selenomethionine-labeled ORF52 (34). Initial growth was carried out at 37 °C until the A_{600} of the culture reached 0.6–0.8 units. The incubation temperature was then decreased to 17 °C, and protein expression was induced by the addition of isopropyl-β-D-thiogalactopyranoside at a final concentration of 1 mM. Following overnight incubation, the cells were harvested by centrifugation.

Selenomethionyl ORF52 was purified using an AKTAxpress (GE Healthcare) based two-step protocol consisting of IMAC (HisTrap HP) and gel filtration (HiLoad 26/60 Superdex 75) chromatography. The purified ORF52 protein was concentrated to 9 mg/ml, flash-frozen in aliquots, and used for crystallization screening. Sample purity (>97%) and molecular mass (12.3 kDa) were verified by SDS-PAGE and matrix-assisted laser desorption-ionization time-of-flight mass spectrometry, respectively.

Crystallization of ORF52—Crystals of ORF52 were obtained by the hanging drop vapor diffusion method at 4 °C. 1 μl of protein solution containing ORF52 in 10 mM Tris, pH 7.5, 100 mM NaCl, and 5 mM dithiothreitol was mixed with 1 μl of the reservoir solution consisting of 80% (v/v) polyethylene glycol 400, 100 mM MOPS, pH 7.0, and 100 mM $NaNO_3$. The crystals were cryo-protected using paratone-n and flash-frozen in liquid propane for data collection at 100 K. They belong to space group *P*2, with cell parameters of $a = 54.9$ Å, $b = 49.2$ Å, $c = 88.9$ Å, and $\beta = 105.6°$. There are two dimers of ORF52 in the asymmetric unit.

Crystals grown in the same crystallization condition but using the mother liquor as cryo-protectant belong to space group *C*2, with cell parameters of $a = 93.5$ Å, $b = 49.4$ Å, $c = 56.4$ Å, and $\beta = 111.9°$. There is one dimer of ORF52 in the crystallographic asymmetric unit.

Structure Determination—A multiple-wavelength anomalous diffraction data set to 2.7 Å resolution was collected at the peak, edge, and remote absorption wavelengths of selenium at the X4A beamline of the National Synchrotron Light Source. The diffraction images were processed with the HKL package (35), and the selenium sites were located with the program BnP (36). The programs SOLVE and RESOLVE (37) were used for phasing the reflections and automated model building, which correctly placed 51% of the residues in the two dimers. An almost complete model of each monomer, except residues 1–6 and 32–38, was built with the program COOT (38) and refined with CNS (39).

TABLE 1
Summary of crystallographic information

Maximum resolution (Å)	2.1
Number of observations	97,958
R_{merge} (%)[a]	6.4 (35.3)
Number of reflections	13,827
Resolution range used in refinement	30–2.1
Completeness (%)	98 (87)
Redundancy	7.1 (5.2)
R factor (%)[b]	21.6 (24.4)
Free *R* factor (%)	23.9 (29.6)
Root mean square deviation in bond lengths (Å)	0.007
Root mean square deviation in bond angles (°)	1.4
Protein Data Bank accession code	2OA5

[a] $R_{merge} = \Sigma_h\Sigma_i|I_{hi} - \langle I_h\rangle|/\Sigma_h\Sigma_i I_{hi}$. The numbers in parentheses are for the highest resolution shell.
[b] $R = \Sigma_h|F_h^o - F_h^c|/\Sigma_h F_h^o$.

A second data set was collected to 2.1 Å and belonged to *C*2 space group. The program COMO (40) was used to solve this structure with a dimer from the *P*2 crystal as the model. The crystallographic information on this model is summarized in Table 1.

Co-immunoprecipitation Experiments—HA-tagged ORF52 was expressed using the pCMV-HA vector (Clontech). Full-length ORF52 and an N-terminal deletion mutant lacking the first 33 residues (ΔN33) were amplified from wild-type MHV-68/BAC by PCR. The R95A single-site mutant of ORF52 was created using an oligonucleotide-directed two-step PCR mutagenesis method. The PCR fragments were cloned into the EcoRI and KpnI sites of pCMV-HA. The clones were verified by sequencing.

293T cells were seeded onto a 6-cm plate (0.8×10^5/plate) 24 h before transfection. 4 μg of HA-tagged expression plasmids for ORF52 or its mutants were individually co-transfected with 4 μg of pFLAG-ORF52 (31) by the calcium phosphate method. 48 h after transfection, the cells were washed once with ice-cold phosphate-buffered saline, and then solubilized in EBC buffer (50 mM Tris-Cl, pH 7.4, 150 mM NaCl, 1% Nonidet P-40, 1 mM EDTA) with protease inhibitors. The lysates were clarified by centrifugation (13,000 rpm, twice for 15 min). Five percent of the supernatant was used as an input control; the rest was incubated overnight at 4 °C with anti-FLAG M2 agarose beads (Sigma) that were washed five times with EBC buffer before use. Immune complexes were washed five times in NETN buffer (20 mM Tris-Cl, pH 8.0, 1 mM EDTA, 0.5% Nonidet P-40, 100 mM NaCl, or 1 M NaCl), and supernatant was depleted. Bound proteins were recovered by boiling in SDS sample buffer for 10 min. Immunoprecipitated proteins were analyzed with primary antibodies specific for HA tag and extracted proteins with antibodies specific for FLAG tag using Western blotting.

Quantitative Real Time PCR—293T cells were seeded onto 24-well plates the day before transfection. 600 ng of BAC (wild-type or 52-null) and 200 ng of plasmid expressing ORF52 or its mutants were co-transfected into each well. After 4 days, the supernatant was collected, and the viral genome was extracted. 200 μl of supernatant was incubated with 100 μg/ml proteinase K and 20 μg/ml RNase A at 37 °C for 15 min, and the reaction was stopped by adding 1/10 volume of 0.5 M EDTA, pH 8.0, followed by incubation at 70 °C for 10 min. An equal volume of 2× lysis buffer (200 mM NaCl, 20 mM Tris-Cl, pH 8.0, 50 mM

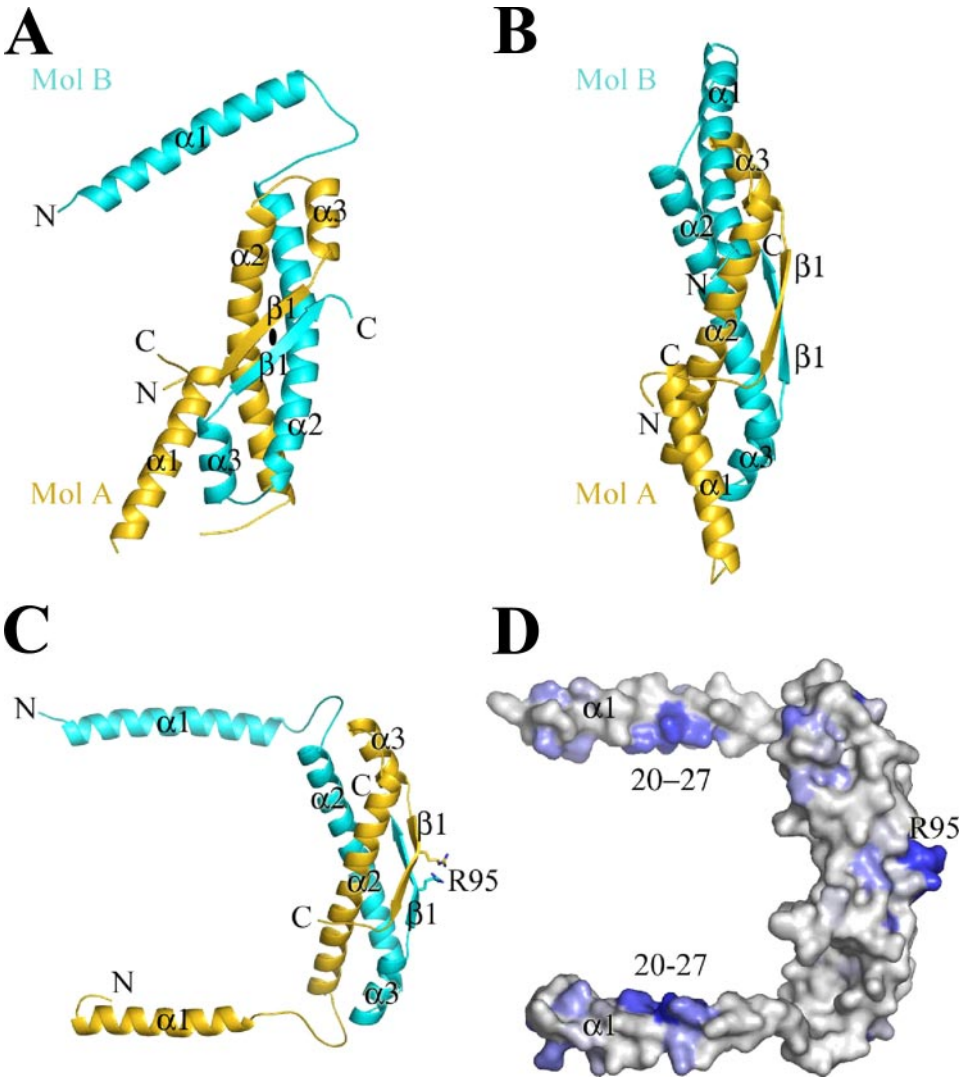

FIGURE 2. **Structure of ORF52 dimer.** *A*, schematic drawing of the ORF52 dimer. Molecule A is shown in *gold*, and molecule B is in *cyan*. *B*, ORF52 dimer after 90° rotation around the vertical axis from *A*. *C*, a model for the ORF52 dimer with the α1 helices splayed away from the rest of the molecules. *D*, conserved molecular surface features of the dimer model, created with ConSurf (43). Residues that are conserved among the herpesviruses are highlighted in *blue* and labeled. *A–C* were created with Pymol (44).

EDTA, pH 8.0) was added, and samples were incubated with shaking at 50 °C for 12–18 h. The samples were extracted twice by phenol/chloroform/isoamyl alcohol (25:24:1), extracted once by chloroform, and then precipitated in ethanol. Extracted genomic DNA was dissolved in 15 μl of TE buffer. Real time PCR was performed on an i-Cycler (Bio-Rad) to determine the viral genome copies in 1 μl of such samples, using SYBR Green and primers that amplify a fragment in MHV-68 ORF65.

RESULTS AND DISCUSSION

Structure Determination—The crystal structure of MHV-68 ORF52 was determined at 2.7 Å resolution by the selenomethionyl multiple-wavelength anomalous diffraction method (41) and refined at 2.1 Å resolution using a second crystal form (Table 1). The structures in the two crystal forms are essentially the same, with root mean square distance of 0.5 Å among their equivalent Cα atoms. The structure at 2.1 Å resolution will be used in further descriptions here. The atomic model has low *R* values and excellent agreement with expected geometric parameters (Table 1). None of the residues of the protein is located in the disallowed region, whereas 97% of the residues are located in the most favored region of the Ramachandran plot (data not shown).

The current atomic model contains residues 6–31 and 41–102 for monomer A and residues 6–102 for monomer B of ORF52 in the crystallographic asymmetric unit. The expression construct covers residues 1–102 of the protein. Additional residues at the C terminus (103–135) are highly hydrophilic in nature and are unlikely to be ordered on their own. A polyethylene glycol 400 (3,6,9,12,15,18,21,24-octaoxahexacosan-1-ol) molecule is bound to each monomer, although they are not related by the 2-fold symmetry of the dimer.

Structure of ORF52 Monomer and Dimer—The structure of ORF52 monomer consists of three α-helices (α1–α3) followed by one β-strand (β1) near the C terminus (Fig. 2*A*). The ORF52 dimer exhibits 2-fold symmetry (except for the N-terminal helix α1; see below) and contains an extensive hydrophobic core between an anti-parallel β-sheet formed by the two β1 strands and the α2 and α3 helices of the two monomers (Fig. 2, *A* and *B*). Approximately 1,900 Å^2 of the surface area of each monomer is buried in the dimer, and residues in this interface are highly conserved among ORF52 homologs (Fig. 1).

Helix α1 at the N terminus does not obey the 2-fold symmetry of the dimer. The helix in monomer A is in contact with the rest of the dimer, but the helix in monomer B is splayed away (Fig. 2*A*). The loop between α1 and α2 is disordered in monomer A. This segment is weakly conserved among ORF52 homologs (Fig. 1). Excluding the α1 helix, the structures of the two monomers are essentially the same, with root mean square distance of 0.5 Å among their equivalent Cα positions.

Structure of ORF52 Tetramer—An asymmetric tetramer of ORF52 is formed from the dimer by the crystallographic 2-fold axis, and the α1 helices of the two dimers are intertwined in this tetramer interface (Fig. 3*A*). The α1 helix that is splayed away from the dimer interacts with the α1 helix that is in contact with the other dimer. The two α1 helices in the tetramer interface are arranged in a parallel fashion and are related by a local 2-fold symmetry operation along their length (Fig. 3*B*). This helix/helix interaction provides most

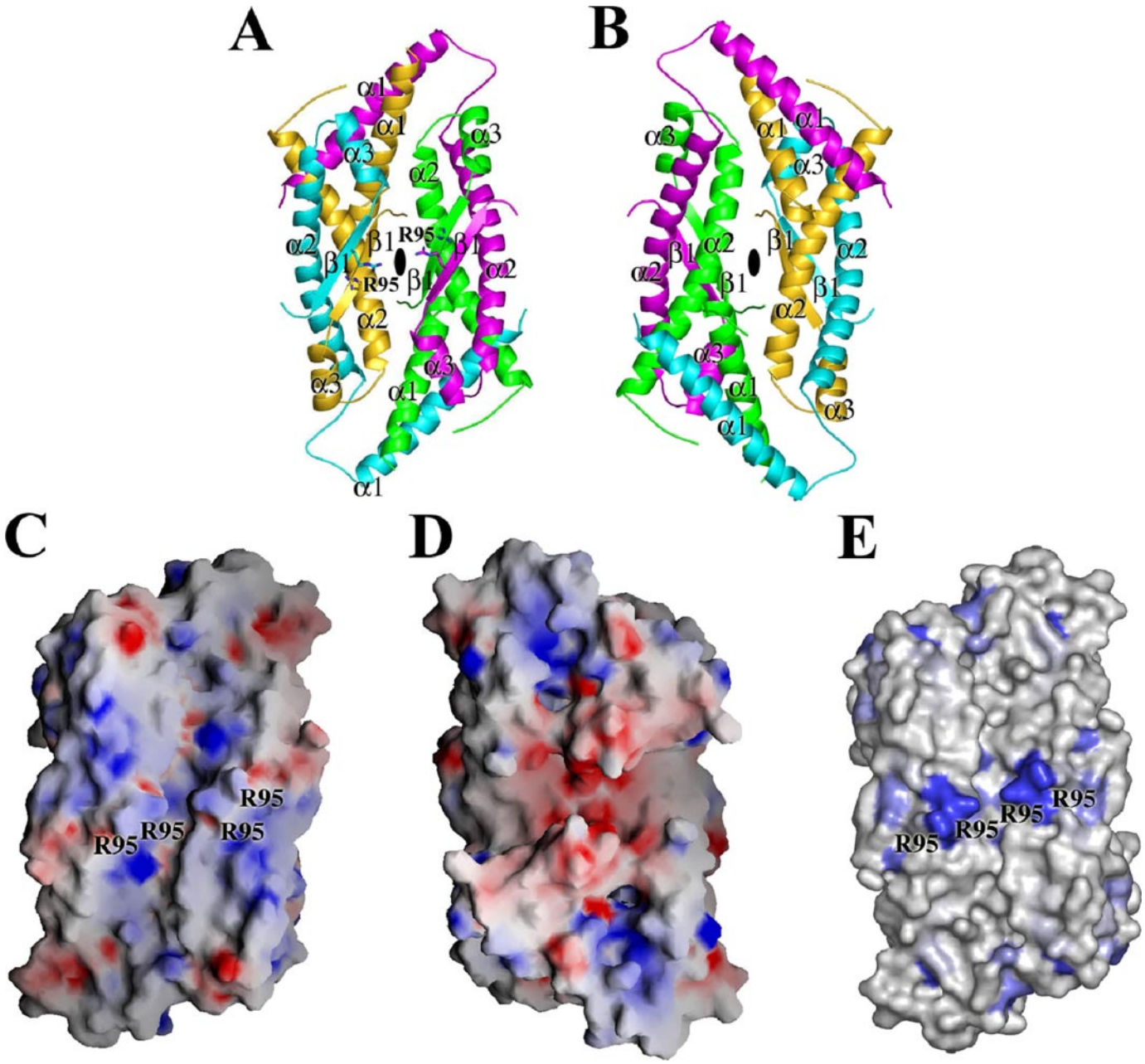

FIGURE 3. **An asymmetric tetramer of ORF52.** *A*, schematic drawing of the ORF52 tetramer. One dimer is shown in *gold* and *cyan*, and other is in *green* and *magenta*. *B*, ORF52 tetramer after 180° rotation around the vertical axis from *A*. *C*, molecular surface of the ORF52 tetramer, in the same view as *A*, colored by electrostatic potentials. *D*, molecular surface of the ORF52 tetramer in the same view as *B*. *E*, conserved molecular surface features of the ORF52 tetramer. *A*, *B*, and *E* created with Pymol (44), and *C* and *D* were created with Grasp (45).

of the 2,500 Å^2 of surface area burial in the tetramer interface. The structural information therefore suggests that this asymmetric tetramer of ORF52 may be stable. Our static light scattering studies showed that ORF52 (residues 1–108) is actually a tetramer in solution.[5]

Several hydrophobic residues are buried at the interface between the α1 helices of the four monomers, including the highly conserved residues Tyr^{10}, Met^{13}, Val^{17}, Leu^{20}, and Leu^{27} (Fig. 1). In addition, Glu^{23} in one monomer is ion-paired with Lys^{28} and hydrogen-bonded to Asn^{24} of the other monomer. These residues are also highly conserved among the ORF52 homologs (Fig. 1). Besides interactions between the α1 helices, several residues from α2 are also located in the tetramer interface, although most of them are hydrophilic in nature (Fig. 1).

Functional Implications—Our structural data suggest two possible models for the active form of ORF52. In one model, ORF52 functions as a dimer (monomers are unlikely to be stable structurally because of the lack of a hydrophobic core). With such a dimer (Fig. 2*C*), the α2 and α3 helices and the β1 strand form a scaffold, and the α1 helix could be projected away from this scaffold to interact with other tegument and/or capsid proteins. The α1 helix is connected to the rest of the protein

[5] J. Benach, Y. Chen, C. Ho, J. Seetharaman, R. Xiao, T. B. Acton, G. T. Montelione, and L. Tong, unpublished data.

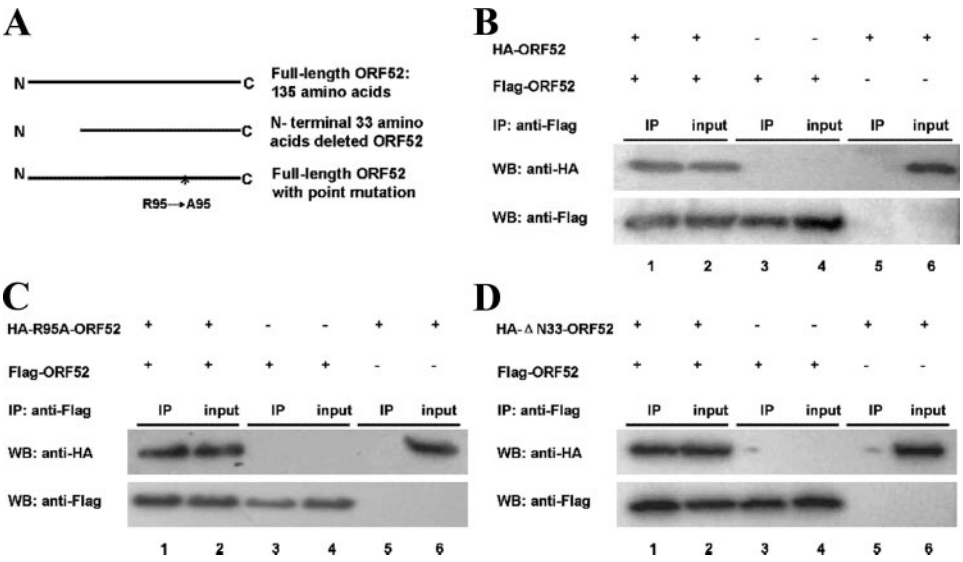

FIGURE 4. **Evidence for ORF52 self-association.** *A*, diagram of the plasmid constructs used in the co-immunoprecipitation (*IP*) study. *B*, co-immunoprecipitation of FLAG-ORF52 and HA-ORF52. *C*, co-immunoprecipitation of FLAG-ORF52 and HA-ORF52ΔN33. *D*, co-immunoprecipitation of FLAG-ORF52 and HA-ORF52/R95A mutant. For *B–D*, lysates were collected from 293T cells co-transfected with FLAG-tagged and HA-tagged ORF52 or its mutants, immunoprecipitated by anti-FLAG antibody, and blotted using anti-HA antibody. Western blotting (*WB*) with anti-FLAG antibody was also performed to check the expression levels of FLAG-ORF52 proteins in transfected cells.

through a long, flexible loop (residues 30–45), which is poorly conserved among ORF52 homologs (Fig. 1). The conformation of α1 observed here is stabilized by the tetramer and may not be the same in the isolated dimer.

This model is supported by the fact that four of the five strictly conserved residues in ORF52 (Leu^{20}, Glu^{23}, Asn^{24}, and Leu^{27}) are located in the α1 helix (Fig. 1). Moreover, several other positions in this helix are conserved to be hydrophobic residues (Met^{13}, Val^{14}, Val^{17}, and Leu^{22}) (Fig. 1). Therefore, once the α1 helix moves away from the rest of the dimer, several conserved, highly hydrophobic patches will be exposed (Fig. 2*D*), which would be optimal for mediating interactions with its partners. The fifth conserved residue, Arg^{95}, is located in strand β1 (Fig. 2*A*). Its side chain is pointed away from the dimer (Fig. 2*D*). In the structure of ORF52, it forms a salt bridge with Asp^{97}, although this residue is not conserved (Fig. 1).

In the second model, ORF52 functions in the tegument as the asymmetric tetramer observed here and interacts with other proteins in the virus. The Arg^{95} residues from the four monomers are clustered together on one face (Fig. 3*C*), although there is a large, electronegative groove in the opposite face of this tetramer (Fig. 3*D*). A possible weakness of this tetramer model is that the only highly conserved surface patch for this tetramer corresponds to that for the Arg^{95} residues (Fig. 3*E*). A larger epitope could be expected to mediate interactions with the other tegument and/or capsid proteins, and such a larger interface is observed in the dimer form of ORF52 (Fig. 2*D*).

Therefore, structural and sequence analyses suggest that the dimer is more likely to be the active form of ORF52, although there are not sufficient experimental data at the current time to distinguish between the two models. On the other hand, the tetramer observed here could be a "latent" form of this protein, *i.e.* the dominant structure in the absence of other protein binding partners. Once ORF52 comes into contact with the proper protein partner, the tetramer will dissociate into dimers, exposing the functional α1 helices. A consistent feature of both models is the functional importance of the α1 helix.

Evidence for ORF52 Self-association in Vivo—Our structural and static light scattering studies show that ORF52 can form dimers and tetramers in solution. We next sought experimental evidence for this self-association *in vivo*, using co-immunoprecipitation experiments. FLAG-tagged wild-type ORF52 and HA-tagged ORF52 and its mutants were co-expressed in 293T cells (Fig. 4*A*). FLAG-ORF52 was immobilized on anti-FLAG agarose, and an anti-HA antibody was used to detect whether the HA-ORF52 was co-immunoprecipitated. Our experiments clearly demonstrate the strong self-association of wild-type ORF52 (Fig. 4*B*). Moreover, mutation of the conserved Arg^{95} residue (Fig. 4*C*) or deletion of the N-terminal 33 residues (Fig. 4*D*), corresponding to removal of helix α1 (Fig. 1), has no effect on this self-association. These observations are in complete agreement with our structural information that the dimeric form of the protein is independent of the α1 helix (Fig. 2*A*). Although the tetrameric form of the protein should be disrupted if helix α1 is deleted (Fig. 3*A*), the co-immunoprecipitation data cannot distinguish between dimers and tetramers of ORF52.

We also employed fluorescence resonance energy transfer assay to confirm the self-interaction of ORF52. We constructed plasmids expressing fusion protein of ORF52 and cyan fluorescent protein (CFP) or yellow fluorescent protein (YFP). The plasmids pCFP/ORF52 and pYFP/ORF52 were either transfected together or alone into 293T cells. Each sample was excited at 415 nm (CFP excitation wavelength), and the fluorescence emission intensity was monitored continuously from 450 to 550 nm. We observed a 1.5-fold decrease of CFP/ORF52 emission intensity in the presence of YFP/ORF52 and a 2-fold increase of YFP/ORF52 emission in the presence of CFP/ORF52 when compared with either CFP/ORF52 or YFP/ORF52 expression alone (data not shown). This result demonstrates a fluorescence energy transfer between CFP/ORF52 and YFP/ORF52 when they are co-expressed, indicating self-interaction of ORF52.

The α1 Helix and Arg^{95} Are Essential for the Function of ORF52—Our structural study suggests that the α1 helix may be essential for the function of ORF52, either mediating interactions with other tegument proteins or driving the formation of the tetramer. To obtain direct experimental evi-

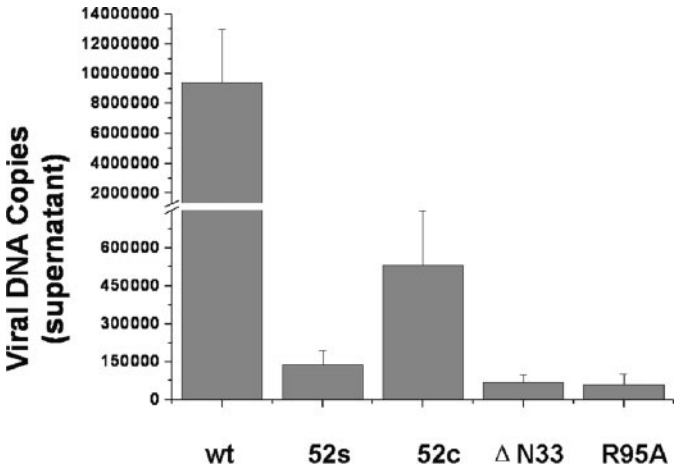

FIGURE 5. **ORF52 mutants do not complement the replication of 52null virus.** 293T cells in 24-well plate were co-transfected with plasmids as follows: wild type (*wt*), 600 ng BAC-7 + 200 ng pcDNA5; 52S, 600 ng BAC-7(52-null) + 200 ng pcDNA5; 52C, 600 ng BAC-7(52-null) + 200 ng pORF52; ΔN33, 600 ng BAC-7(52-null) + 200 ng pORF52ΔN33; and R95A, 600 ng BAC-7(52-null) + 200 ng pORF52-R95A. Four days after transfection, viral genomes were extracted from the supernatant, and genome copies were analyzed through quantitative real time PCR.

dence for the functional importance of this helix, we assessed the ability of a deletion mutant lacking these N-terminal residues in rescuing an *ORF52-null* mutant virus. An *ORF52-null* MHV-68/BAC mutant (31) was co-transfected into 293T cells with a wild-type or mutant ORF52 expression plasmid. Four days later, viral particles were collected from supernatants, and viral genomes were extracted and subjected to quantitative real time PCR analysis to examine the ability of each mutant ORF52 to complement the *ORF52-null* MHV-68/BAC mutant in tegumentation and egress of mature viral particles. Although the wild-type ORF52 can readily rescue the mutant phenotype and lead to the production of a large amount of virus particles, the deletion mutant lacking helix α1 cannot rescue the ORF52-null virus (Fig. 5). In addition, the conserved Arg^{95} residue is also essential for the function of the protein, because the R95A mutant cannot rescue the ORF52-null virus (Fig. 5).

In summary, we have determined the crystal structure of the abundant tegument protein ORF52 of MHV-68 at 2.1 Å resolution. Structural and sequence analyses suggest that an N-terminal α-helix may be essential for the functions of this protein, which has been confirmed by mutagenesis and functional studies *in vivo*. This helix may mediate the interactions between ORF52 and other proteins in the tegument and/or capsid of MHV-68. Efforts at identifying these protein partners of ORF52 are currently in progress.

Acknowledgments—We thank John Schwanof and Randy Abramowitz for setting up the X4A beamline.

REFERENCES

1. Mettenleiter, T. C. (2002) *J. Virol.* **76,** 1537–1547
2. Roizman, B., and Knipe, D. M. (2001) in *Fields Virology* (Knipe, D. M., Howley, P. M., Griffin, R. A., Lamb, R. A., Martin, M. A., Roizman, B., and Straus, S. E., eds) 4th Ed., pp. 2399–2459, Lippincott Williams & Wilkins, Philadelphia, PA
3. Subak-Sharpe, J. H., and Dargan, D. J. (1998) *Virus Genes* **16,** 239–251
4. Bresnahan, W. A., and Shenk, T. E. (2000) *Proc. Natl. Acad. Sci. U. S. A.* **97,** 14506–14511
5. Castillo, J. P., and Kowalik, T. F. (2002) *Gene* (*Amst.*) **290,** 19–34
6. Ishov, A. M., Vladimirova, O. V., and Maul, G. G. (2002) *J. Virol.* **76,** 7705–7712
7. Zhu, F. X., King, S. M., Smith, E. J., Levy, D. E., and Yuan, Y. (2002) *Proc. Natl. Acad. Sci. U. S. A.* **99,** 5573–5578
8. Bortz, E., Whitelegge, J. P., Jia, Q., Zhou, Z. H., Stewart, J. P., Wu, T. T., and Sun, R. (2003) *J. Virol.* **77,** 13425–13432
9. Britt, W. J., and Boppana, S. (2004) *Hum. Immunol.* **65,** 395–402
10. Kattenhorn, L. M., Mills, R., Wagner, M., Lomsadze, A., Makeev, V., Borodovsky, M., Ploegh, H. L., and Kessler, B. M. (2004) *J. Virol.* **78,** 11187–11197
11. Varnum, S. M., Streblow, D. N., Monroe, M. E., Smith, P., Auberry, K. J., Pasa-Tolic, L., Wang, D., Camp II, D. G., Rodland, K., Wiley, S., Britt, W. J., Shenk, T. E., Smith, R. D., and Nelson, J. A. (2004) *J. Virol.* **78,** 10960–10966
12. Johannsen, E., Luftig, M., Chase, M. R., Weicksel, S., Cahir-McFarland, E., Illanes, D., Sarracino, D., and Kieff, E. (2004) *Proc. Natl. Acad. Sci. U. S. A.* **101,** 16286–16291
13. O'Connor, C. M., and Kedes, D. H. (2006) *J. Virol.* **80,** 1574–1583
14. Knipe, D. M., and Howley, P. M. (2001) *Fields Virology*, pp. 2511–2574, Lippincott Williams & Wilkins, Philadelphia, PA
15. Blasdell, K., McCracken, C., Morris, A., Nash, A. A., Begon, M., Bennett, M., and Stewart, J. P. (2003) *J. Gen. Virol.* **84,** 111–113
16. Mistrikova, J., and Blaskovic, D. (1985) *Acta Virol.* **29,** 312–317
17. Rajcani, J., Blaskovic, D., Svobodova, J., Ciampor, F., Huckova, D., and Stanekova, D. (1985) *Acta Virol.* **29,** 51–60
18. Efstathiou, S., Ho, Y. M., Hall, S., Styles, C. J., Scott, S. D., and Gompels, U. A. (1990) *J. Gen. Virol.* **71,** 1365–1372
19. Nash, A. A., Usherwood, E. J., and Stewart, J. P. (1996) *Semin. Virol.* **7,** 125–130
20. Speck, S. H., and Virgin, H. W. (1999) *Curr. Opin. Microbiol.* **2,** 403–409
21. Simas, J. P., and Efstathiou, S. (1998) *Trends Microbiol.* **6,** 276–282
22. Adler, H., Messerle, M., Wagner, M., and Koszinowski, U. H. (2000) *J. Virol.* **74,** 6964–6974
23. Borst, E. M., Hahn, G., Koszinowski, U. H., and Messerle, M. (1999) *J. Virol.* **73,** 8320–8329
24. Delecluse, H. J., Hilsendegen, T., Pich, D., Zeidler, R., and Hammerschmidt, W. (1998) *Proc. Natl. Acad. Sci. U. S. A.* **95,** 8245–8250
25. Smith, G. A., and Enquist, L. W. (1999) *J. Virol.* **73,** 6405–6414
26. Song, M. J., Hwang, S., Wong, W. H., Wu, T. T., Lee, S., Liao, H. I., and Sun, R. (2005) *Proc. Natl. Acad. Sci. U. S. A.* **102,** 3805–3810
27. Ebrahimi, B., Dutia, B. M., Roberts, K. L., Garcia-Ramirez, J. J., Dickinson, P., Stewart, J. P., Ghazal, P., Roy, D. J., and Nash, A. A. (2003) *J. Gen. Virol.* **84,** 99–109
28. Martinez-Guzman, D., Rickabaugh, T., Wu, T. T., Brown, H., Cole, S., Song, M. J., Tong, L., and Sun, R. (2003) *J. Virol.* **77,** 10488–10503
29. Fuchs, W., Granzow, H., Klupp, B. G., Kopp, M., and Mettenleiter, T. C. (2002) *J. Virol.* **76,** 6729–6742
30. Mettenleiter, T. C. (2004) *Virus Res.* **106,** 167–180
31. Bortz, E., Wang, L., Jia, Q., Wu, T. T., Whitelegge, J. P., Deng, H., Zhou, Z. H., and Sun, R. (2007) *J. Virol.* **81,** 10137–10150
32. Acton, T. B., Gunsalus, K., Xiao, R., Ma, L., Aramini, J., Baron, M. C., Chiang, Y., Clement, T., Cooper, B., Denissova, N., Douglas, S., Everett, J. K., Palacios, D., Paranji, R. H., Shastry, R., Wu, M., Ho, C.-H., Shih, L., Swapna, G. V. T., Wilson, M., Gerstein, M., Inouye, M., Hunt, J. F., and Montelione, G. T. (2005) *Methods Enzymol.* **394,** 210–243
33. Jansson, M., Li, Y.-C., Jendeberg, L., Anderson, S., Montelione, G. T., and Nilsson, B. (1996) *J. Biomol. NMR* **7,** 131–141
34. Doublie, S., Kapp, U., Aberg, A., Brown, K., Strub, K., and Cusack, S. (1996) *FEBS Lett.* **384,** 219–221
35. Otwinowski, Z., and Minor, W. (1997) *Method Enzymol.* **276,** 307–326
36. Weeks, C. M., Adams, P. D., Berendzen, J., Brunger, A. T., Dodson, E. J., Grosse-Kunstleve, R. W., Schneider, T. R., Sheldrick, G. M., Terwilliger, T. C., Turkenburg, M. G., and Uson, I. (2003) *Methods Enzymol.* **374,** 37–83

37. Terwilliger, T. C. (2003) *Methods Enzymol.* **374,** 22–37
38. Emsley, P., and Cowtan, K. D. (2004) *Acta Crystallogr. Sect. D Biol. Crystallogr.* **60,** 2126–2132
39. Brunger, A. T., Adams, P. D., Clore, G. M., DeLano, W. L., Gros, P., Grosse-Kunstleve, R. W., Jiang, J.-S., Kuszewski, J., Nilges, M., Pannu, N. S., Read, R. J., Rice, L. M., Simonson, T., and Warren, G. L. (1998) *Acta Crystallogr. Sect. D Biol. Crystallogr.* **54,** 905–921
40. Jogl, G., Tao, X., Xu, Y., and Tong, L. (2001) *Acta Crystallogr. Sect. D Biol. Crystallogr.* **57,** 1127–1134
41. Hendrickson, W. A. (1991) *Science* **254,** 51–58
42. Gouet, P., Courcelle, E., Stuart, D. I., and Metoz, F. (1999) *Bioinformatics* **15,** 305–308
43. Armon, A., Graur, D., and Ben-Tal, N. (2001) *J. Mol. Biol.* **307,** 447–463
44. DeLano, W. L. (2002) *PyMol Manual*, DeLano Scientific, San Carlos, CA
45. Nicholls, A., Sharp, K. A., and Honig, B. (1991) *Proteins* **11,** 281–296